Coupled interaction between unsteady flame dynamics and acoustic field in a turbulent combustor

Vedasri Godavarthi,[1,a)] Samadhan A. Pawar,[1] Vishnu R. Unni,[1] R. I. Sujith,[1] Nobert Marwan,[2] and Jürgen Kurths[2,3,4]

[1]*Department of Aerospace Engineering, Indian Institute of Technology Madras, 600036 Chennai, India*
[2]*Potsdam Institute for Climate Impact Research, P.O. Box 601203, 14412 Potsdam, Germany*
[3]*Department of Physics, Humboldt University, Newtonstr. 15, 12489 Berlin, Germany*
[4]*Institute for Complex Systems and Mathematical Biology,University of Aberdeen, Aberdeen AB243UE, United Kingdom*

(Received 15 August 2018; accepted 22 October 2018; published online 14 November 2018)

Thermoacoustic instability is a result of the positive feedback between the acoustic pressure and the unsteady heat release rate fluctuations in a combustor. We apply the framework of the synchronization theory to study the coupled behavior of these oscillations during the transition to thermoacoustic instability in a turbulent bluff-body stabilized gas-fired combustor. Furthermore, we characterize this complex behavior using recurrence plots and recurrence networks. We mainly found that the correlation of probability of recurrence (*CPR*), the joint probability of recurrence (*JPR*), the determinism (*DET*), and the recurrence rate (*RR*) of the joint recurrence matrix aid in detecting the synchronization transitions in this thermoacoustic system. We noticed that *CPR* and *DET* can uncover the occurrence of phase synchronization state, whereas *JPR* and *RR* can be used as indices to identify the occurrence of generalized synchronization (GS) state in the system. We applied measures derived from joint and cross recurrence networks and observed that the joint recurrence network measures, transitivity ratio, and joint transitivity are useful to detect GS. Furthermore, we use the directional property of the network measure, namely, cross transitivity to analyze the type of coupling existing between the acoustic field (p') and the heat release rate ($\dot{q}'$) fluctuations. We discover a possible asymmetric bidirectional coupling between $\dot{q}'$ and p', wherein $\dot{q}'$ is observed to exert a stronger influence on p' than vice versa. *Published by AIP Publishing.* https://doi.org/10.1063/1.5052210

In practical combustion systems, a positive coupling between the acoustic field and the unsteady heat release rate fluctuations results in the occurrence of ruinously large amplitude acoustic oscillations, commonly referred to as the thermoacoustic instability. Recently, many studies have been conducted to investigate the transition to such instabilities from a state of combustion noise (stable state composed of low amplitude aperiodic oscillations) to thermoacoustic instability. As thermoacoustic instability is a result of coupled behavior between the acoustic pressure and the heat release rate, synchronization theory has been introduced to quantify the coupling between them. Pawar *et al.*[25] have found that the periodic oscillations exhibited during the state of thermoacoustic instability are of two types, namely, weakly correlated and strongly correlated limit cycle oscillations. The difference between these states can be attributed to the extent of coupling that exists between the heat release rate and the acoustic oscillations in the system. Hence, it is important to characterize the synchronization transition to thermoacoustic instability in order to detect the occurrence of these dynamical states and also the directional dependence between these oscillations. We apply measures derived from recurrence plots and recurrence networks to detect the synchronization transition observed during the onset of thermoacoustic instability. Furthermore, we characterize the directional dependence between the acoustic field and the heat release rate fluctuations using measures derived from the cross recurrence networks constructed from their time series.

I. INTRODUCTION

Thermoacoustic instability comprises of large amplitude periodic oscillations, which can arise due to the positive coupling between the acoustic field (p') and the heat release rate ($\dot{q}'$) fluctuations in a combustor.[1–3] The mutual interaction between these subsystems results in the transition of the system behavior from a stable (combustion noise) to an unstable (thermoacoustic instability) operation. Even though thermoacoustic instability corresponds to the state of stable limit cycle oscillations, the occurrence of such an instability can lead to undesirable effects, such as loss of engine performance, structural damage of the engine components, or sometimes failure of missions.[6,7] Hence, thermoacoustic instability corresponds to unstable operation regime of the engine.[4,5] The investigation of the transition to thermoacoustic instability is therefore important. Over the years, various studies have been performed either to predict[8–10] or to control[11–14] the occurrence of such instabilities.

The onset of thermoacoustic instability is a nonlinear phenomenon.[15,16] The nonlinearity arises primarily due to the interaction between the acoustic field and the heat release rate oscillations in a combustor.[17] Various studies have used

a)Author to whom correspondence should be addressed: vedasrigodavarthi@gmail.com

the approach of dynamical systems theory to characterize the nonlinear behavior of the thermoacoustic systems and also to detect the dynamical transitions observed prior to the onset of thermoacoustic instability. With the help of dynamical systems approach, a rich dynamical behavior has been reported during the transition to thermoacoustic in such systems.[8,10,16,18–20] Kabiraj *et al.*[20] showed the existence of various dynamical states such as quasiperiodic, chaotic, and period-k, in addition to limit cycle oscillations (LCO), in a premixed laminar thermoacoustic system.

Recently, there have been many investigations focusing on characterizing the underlying dynamics observed during the transition to thermoacoustic instability.[1,18,21–24] In most of the turbulent combustors, as the equivalence ratio is varied from stoichiometric to fuel lean regimes, a transition in the system dynamics from low amplitude aperiodic oscillations (combustion noise) to large amplitude LCO (thermoacoustic instability) is observed. Traditionally, combustion noise was considered as mere stochastic fluctuations in the system. Nair *et al.*[26] and Tony *et al.*[27] used a plethora of tools to ascertain the deterministic nature of the signal and discovered that combustion noise has features of high dimensional chaotic oscillations contaminated with coloured and white noise. Nair and Sujith[28] detected the presence of multifractality during combustion noise. Furthermore, they described the transition from combustion noise to thermoacoustic instability as a transition from chaos to order, which is reflected as the loss of multifractality in the pressure fluctuations. Nair *et al.*[8] also reported that the onset of thermoacoustic instability is preceded by a state called intermittency, which is composed of bursts of large amplitude periodic oscillations appearing amidst the low amplitude aperiodic oscillations at irregular intervals.

The characterization of the dynamics en route to thermoacoustic instability is required for its prognosis and control. Various tools derived from the nonlinear time series analysis and complex networks were used to detect the transition to thermoacoustic instability.[16] Nair and Sujith[28] and Unni and Sujith[29] demonstrated that the Hurst exponent can be used as an early warning measure for thermoacoustic instability and blowout. In their subsequent work,[8] they used recurrence quantification analysis on time series of acoustic pressure and found that recurrence measures can be used as precursors. Unni *et al.*[30] applied an anomaly measure from symbolic time series analysis to detect the onset of thermoacoustic instability. Recently, researchers[31–33] used tools from complex network theory and demonstrated that the measures derived from visibility graphs and recurrence networks can be used as early warning signals to thermoacoustic instability and blowout. However, none of the above analysis investigated the coupled behavior of p' and $\dot{q}'$.

It is well known that the coupled interaction between p' and $\dot{q}'$ causes thermoacoustic instability.[34] Various studies in the past have focused on this coupled interaction during either the stable or the unstable regimes of combustor operation.[35–45] Recently, such coupled interaction between p' and $\dot{q}'$ at various dynamical states during the transition from combustion noise to thermoacoustic instability via intermittency was analyzed by Pawar *et al.*[25] and Mondal *et al.*[22]

Pawar *et al.*[25] applied the synchronization framework to characterize the temporal behavior of the coupled p' and $\dot{q}'$ in a turbulent combustor. They cast the chamber acoustic field (p') and the turbulent reactive flow ($\dot{q}'$) as oscillators to apply the synchronization framework to the thermoacoustic system, as these oscillators exhibit self-sustained oscillations under the influence of a turbulent flow (see the Appendix for more details). Using tools from synchronization theory, they described that the transition to thermoacoustic instability happens from a state of desynchronized aperiodicity (combustion noise) to the states of phase synchronized (PS) and generalized synchronized (GS) periodic oscillations. Such a transition to PS is observed to occur via a state of intermittent phase synchronization (IPS). However, in their study, the characterization of these states was mostly qualitative. The characterization of spatiotemporal behavior of the coupled acoustic field and local heat release rate fluctuations in the reaction field during the intermittency route to thermoacoustic instability was performed by Mondal *et al.*[22] They observed that the transition from combustion noise (phase asynchronous state) to thermoacoustic instability (phase synchronous state) occurs through the formation of a chimera-like state where the phase asynchronous and the phase synchronous regions coexist at the same instance in the reaction field. They observed that the Kuramoto order parameter indicates the synchronization transition at the onset of thermoacoustic instability. Chiocchini *et al.*[46] characterized the nature of coupling between p' and $\dot{q}'$ during the onset of thermoacoustic instability. They reported that a chaotic synchronization index, namely, interdependence index, can detect the onset of thermoacoustic instability. They also found that the dependence of p' on $\dot{q}'$ is higher than vice versa and that the heat release rate acts as a driving subsystem. They suggested that, while the asymmetry in the interdependence index implied the presence of an unidirectional coupling between p' and $\dot{q}'$, in reality this cannot be true. They attributed this anomaly to the difference in intrinsic embedding dimensions of the pressure and the heat release rate oscillations which cannot be accommodated in the computation of the interdependence index. We hypothesize that this anomaly observed due to interdependence index is not merely because of the difference in intrinsic embedding dimensions, but might also be due to the asymmetric bidirectional coupling between acoustic pressure and unsteady heat release rate. Hence, there exists a need for a detailed quantitative analysis to detect the synchronization transition and for the characterization of the directional dependence between p' and $\dot{q}'$, which we intend to address in this paper.

We apply measures based on the recurrences in the reconstructed phase space of p' and $\dot{q}'$ to characterize the synchronization transition observed during the transition to thermoacoustic instability in a bluff body stabilized turbulent flame combustor. The synchronization measures[47] derived from the probability of recurrence plot, such as the correlation of probability of recurrence (*CPR*) and the joint probability of recurrence (*JPR*), are used to detect the PS and GS states, respectively. We also apply recurrence quantification analysis on the joint recurrence matrix, a matrix encoding information

regarding the simultaneous occurrence of recurrences in both the systems, and observe that the recurrence rate (*RR*) and the determinism (*DET*) can detect the occurrence of the GS and PS states, respectively, in our system. The geometric detection of coupling is performed using networks constructed from the joint recurrence and cross recurrence plots. Using the measures of joint transitivity and transitivity ratio introduced by Feldhoff *et al.*,[48] we identify a GS state. In order to determine the directional dependence between p' and $\dot{q}'$, the network measure cross transitivity, introduced by Feldhoff *et al.*,[49] is computed. We discover an existence of a possible asymmetric bidirectional coupling between p' and $\dot{q}'$ and observe that $\dot{q}'$ exerts a stronger influence on p' than vice versa.

In Sec. II, we describe the measures used for quantification in this paper. The experimental setup is presented in Sec. III. The results are discussed in Sec. IV, and the conclusions are given in Sec. V.

II. RECURRENCE BASED SYNCHRONIZATION ANALYSIS

Recurrence is a fundamental property of any deterministic dynamical system.[50] Recurrences are visualized using a recurrence plot constructed from a recurrence matrix. The recurrences are computed after reconstructing the phase space from a measured time series using Takens' embedding theorem.[51] The delayed vectors are constructed from the discrete time samples $x_1, x_2, \ldots x_N$ using an optimum time delay (d) and an optimum embedding dimension (M). Thus, the ith delay vector is given by

$$V_i = x_i, x_{i+d}, x_{i+2d} \ldots x_{i+(M-1)d}. \tag{1}$$

In this paper, the time delay (d) is chosen as the first minimum of the average mutual information (AMI), and the embedding dimension is detected using Cao's method.[52]

In order to compute the recurrences of the phase space trajectories, the Euclidean distance between two delay vectors is computed, and if the distance $\|V_i - V_j\|$ is less than the recurrence threshold ϵ_V, we say that the state V_i is recurrent. These recurrences are stored in the recurrence matrix R

$$R_{ij} = \Theta(\epsilon_V - \|V_i - V_j\|), \tag{2}$$

where Θ is the Heaviside function. The recurrence matrix comprises 0s and 1s. If an element of the recurrence matrix is 1, then the corresponding state is recurrent; otherwise, it is not. For the present study, we select a threshold (ϵ_V) in such a way that the recurrence rate (described in Sec. II A) is fixed.

The coupled behavior of two oscillators is studied using the multivariate recurrence matrices.[53] The univariate recurrence matrix R can be extended as joint and cross recurrence matrices to study the coupled behavior of the oscillators.

The joint recurrence matrix (*JRM*) is computed by the element-wise multiplication of the individual recurrence matrices (R^X, R^Y) of the two oscillators X and Y. If the delay vectors of the two oscillators are denoted by V and W, respectively, then

$$JRM_{ij} = \Theta(\epsilon_V - \|V_i - V_j\|)\Theta(\epsilon_W - \|W_i - W_j\|). \tag{3}$$

JRM captures the presence of simultaneous recurrences of the phase trajectories of both the oscillators. If the states V_i and W_i recur simultaneously, then $JRM_{ij} = 1$; otherwise, $JRM_{ij} = 0$.

The cross recurrence matrix (*CRM*) compares the states of the two oscillators in the same reconstructed phase space and is computed as follows:

$$CRM_{ij} = \Theta(\epsilon_{VW} - \|V_i - W_j\|). \tag{4}$$

CRM captures the presence of similar states in both the oscillators. If $CRM_{ij} = 1$, then the state of one oscillator recurs to the state of the other oscillator. Unlike R and *JRM*, the *CRM* is not necessarily symmetric. The threshold (ϵ_{VW}) is chosen such that the cross recurrence rate is fixed.

In order to link the recurrent behavior of two oscillators to detect synchronization between them, a measure of probability of recurrence $P(\tau)$, also referred to as τ—recurrence rate, was introduced by Romano *et al.*[47] $P(\tau)$ measures the probability with which a given state vector of the trajectory of a single oscillator recurs after a time lag τ,

$$P(\tau) = \frac{1}{N-\tau}\sum_{i=1}^{N-\tau}\Theta(\epsilon_V - \|V_i - V_j\|). \tag{5}$$

The type of synchronization is characterized based on the locking of the location of the peaks as well as their heights in the $P(\tau)$ plots of the two oscillators. Further details on the use of probability of recurrence plots to detect the synchronization states in the thermoacoustic system are given in Pawar *et al.*[25]

A. Measures to quantify the coupled behavior of oscillators using recurrence plots

1. Determinism (DET)

Determinism (*DET*) measures the percentage of recurrence points in a recurrence matrix which form diagonal lines of minimum length l_{min},

$$DET = \frac{\sum_{l=l_{min}}^{N} lF(l)}{\sum_{l=1}^{N} lF(l)}, \tag{6}$$

where $F(l)$ is the frequency distribution of the lengths of the diagonal lines and N is the number of state vectors in the reconstructed phase space. When the dynamics is periodic, RP comprises only diagonal lines, and hence, *DET* attains the maximum value of 1. Thus, *DET* can be used to detect the occurrence of periodic and quasiperiodic dynamics in the system.

2. Recurrence rate (RR)

Recurrence rate (*RR*) measures the average number of recurrences present in a recurrence matrix, R

$$RR = \frac{1}{N^2}\sum_{i,j=1}^{N} R_{ij}. \tag{7}$$

RR attains the maximum value of 1 when all the state vectors are recurring in the reconstructed phase space. We fix *RR* of the recurrence matrices of p' and $\dot{q}'$ to compare across different states.

3. Correlation of probability of recurrence (CPR)

Correlation of probability of recurrence (*CPR*) is the cross correlation of the probability of recurrences of the two oscillators,

$$CPR = \frac{\langle \bar{P}_1(\tau > \tau_c)\bar{P}_2(\tau > \tau_c)\rangle}{\sigma_1\sigma_2}. \quad (8)$$

Here, $\bar{P}_1$ and $\bar{P}_2$ are the mean subtracted values of P_1 and P_2, and σ_1, σ_2 are the standard deviations of $\bar{P}_1(\tau)$ and $\bar{P}_2(\tau)$, respectively. We use the modified form of *CPR* proposed by Goswami *et al.*[54] and consider only those lags (τ) which are greater than the lag (τ_c) at which the autocorrelation of the signal is lesser than $1/e$ to exclude the effect of autocorrelation. The value of *CPR* ranges between -1 and 1. If both the oscillators are phase synchronized, then the location of the peaks of both $P_1(\tau)$ and $P_2(\tau)$ coincide. Hence, the *CPR* reaches its maximum (closer to 1) and can be used as an index to detect PS.[47]

4. Joint probability of recurrence (JPR)

Joint probability of recurrence (*JPR*) is the average probability of joint recurrences in time, whose value can be obtained as follows:

$$JPR = \frac{\frac{RR_J}{RR} - RR}{1 - RR}, \quad (9)$$

where RR_J is the joint recurrence rate and *RR* is the recurrence rate of the individual recurrence matrices. The joint recurrence rate is given by

$$RR_J = \frac{1}{N^2}\sum_{i,j=1}^{N} JRM_{ij}. \quad (10)$$

During the regime of generalized synchronization (GS), we expect a similar value of RR_J as that of individual *RR* of both the oscillators. Hence, *JPR* becomes closer to 1 during the GS state and can be used as an index to detect the GS state.[47]

All the above measures are based on the individual and joint recurrence matrices computed from the time series of coupled oscillators. We now describe measures derived from the joint and cross recurrence networks. These networks are based on geometric signatures of the attractors in the phase space.

B. Measures to quantify the coupled behavior using recurrence networks

We construct recurrence networks from recurrence matrices.[55] The adjacency matrix (A_{ij}) is computed from R_{ij} as follows:

$$A_{ij} = R_{ij} - I_{ij}, \quad (11)$$

where I_{ij} is the identity matrix, i.e., we subtract the identity matrix from the *R* to discount self connected nodes in the network. The nodes in the recurrence network correspond to the state vectors in the reconstructed phase space. Two states are connected with a link, if they recur.

For studying the coupled behavior of two oscillators, networks are constructed from *JRM* and *CRM*, respectively. The measures computed from the recurrence networks are described below.

1. Network transitivity ($\mathcal{T}$)

Network transitivity computes the number of closed triangles in a network given that two among those three nodes are connected,[56]

$$\mathcal{T} = \frac{\sum_{i,j,k=1}^{N} A_{ij}A_{jk}A_{ki}}{\sum_{i,j,k=1}^{N} A_{ij}.A_{jk}}. \quad (12)$$

In order to study the coupled behavior of two oscillators, the joint transitivity ($\mathcal{T}_J$) is used, which is the transitivity of the joint recurrence network. During GS, $\mathcal{T}_J$ is high due to the increase in the occurrence of simultaneous recurrences. Feldhoff *et al.*[48] introduced a normalized measure, the transitivity ratio ($Q_{\mathcal{T}}$), which is the ratio of joint transitivity to the individual transitivities, and $\mathcal{T}_X$ and $\mathcal{T}_Y$ of the two oscillators *X* and *Y*,

$$Q_{\mathcal{T}} = \frac{2\mathcal{T}_J}{\mathcal{T}_X + \mathcal{T}_Y}. \quad (13)$$

Here, $Q_{\mathcal{T}}$ will reach its maximum (around 1) during the occurrence of GS and hence can be used as an index to detect GS.

2. Cross transitivity

Cross transitivity, $\mathcal{T}_{XY}$, is the probability that two nodes in the recurrence network of the second oscillator (*Y*) are connected given that they are neighbors to a node in the recurrence network of the first oscillator (*X*). In other words, it measures the number of triangles with two vertices in one network and the third vertex in the other network.[49] The interlinks between the two networks are obtained using *CRM*. *CRM* is not necessarily symmetric, and hence, $\mathcal{T}_{XY}$ need not be the same as $\mathcal{T}_{YX}$. This inequality can be used to characterize the directional dependence of the two oscillators.[49]

III. EXPERIMENTAL SETUP

The time series of p' and $\dot{q}'$ analyzed here are acquired from a backward facing step turbulent flame combustor. The flame stabilizing mechanism used is a bluff body whose diameter and thickness are 47 mm and 10 mm, respectively. The cross section area of the combustor is $90 \times 90\ \text{mm}^2$. The bluff body is positioned at 45 mm from the dump plane inside the combustor. Liquid petroleum gas (LPG) is injected at 120 mm upstream of the bluff body, and a spark plug positioned at the dump plane is used for ignition. The air and fuel flow rates are controlled separately by using mass flow controllers (Alicat Scientific MCR-2000 slpm for air and MCR-100 slpm for fuel). The uncertainty of the mass flow controllers is $\pm$(0.8% of reading + 0.2% of full scale). A constant fuel flow rate of 25 slpm is maintained, while the air flow rate is varied from 400 slpm to 940 slpm. This in turn varies the Reynolds number (*Re*) from 1.09×10^5 to 2.12×10^5. The uncertainties in *Re* are $\pm1.97\times10^3$ to $\pm2.71\times10^3$. The respective equivalence ratios vary from 0.95 ± 0.02 to 0.46 ± 0.01. The mean flow velocities ($\bar{u}$) vary from 9.2 m/s to 18.1 m/s. The estimated uncertainties in $\bar{u}$ are from $\pm$0.16 m/s to $\pm$0.22 m/s. The

pressure measurements are performed using a PCB103B02 piezoelectric transducer with an uncertainty of ±0.15 Pa. The unsteady heat release rate fluctuations in terms of CH* chemiluminescence intensity are captured using a photomultiplier tube (PMT; Hamamatsu H10722-01) equipped with a CH* bandpass filter ($\lambda = 432$ nm and 10 nm full width at half maximum). The pressure and heat release rate fluctuations are measured for a duration of 3 s and sampled at a frequency of 10 kHz. The detailed description of the experimental setup and the uncertainties involved are given in Pawar *et al.*[25] and Unni and Sujith.[29]

IV. RESULTS AND DISCUSSIONS

The transition of the system dynamics from a stable operation (combustion noise) to an unstable one (thermoacoustic instability) occurs when the equivalence ratio is decreased from a value close to stoichiometry to a fuel lean condition due to an increase in the mean flow velocity $\bar{u}$. In this study, the flow velocity is varied from 9.2 m/s to 18.1 m/s. The time series of p' and $\dot{q}'$ are plotted in Fig. 1.

When the flow velocity is 9.2 m/s, we observe low amplitude aperiodic oscillations in both p' and $\dot{q}'$ [Fig. 1(a)]. This state is called combustion noise. We observe that p' and $\dot{q}'$ oscillate independently during this state. As $\bar{u}$ increases from 9.2 m/s to 11.9 m/s, we observe a transition from combustion noise to intermittency. During intermittency, there are bursts of periodic oscillations occurring at random intervals amidst epochs of aperiodic oscillations [Fig. 1(b)]. We find that p' and $\dot{q}'$ appear to be locked during the bursts of periodic oscillations, and they appear to oscillate independently during the aperiodic epochs of oscillations. When $\bar{u}$ increases to 12.5 m/s, we observe the occurrence of weakly correlated LCO [Fig. 1(c)]. During this state, there is a wide variation in the cycle-to-cycle amplitude of both the signals, while their phases appear to be locked in time. A further increase in $\bar{u}$ to 16.2 m/s leads to a transition from this weakly correlated LCO to a strongly correlated LCO [Fig. 1(d)]. During this state, both the phases as well as the amplitudes appear to be highly correlated in time.

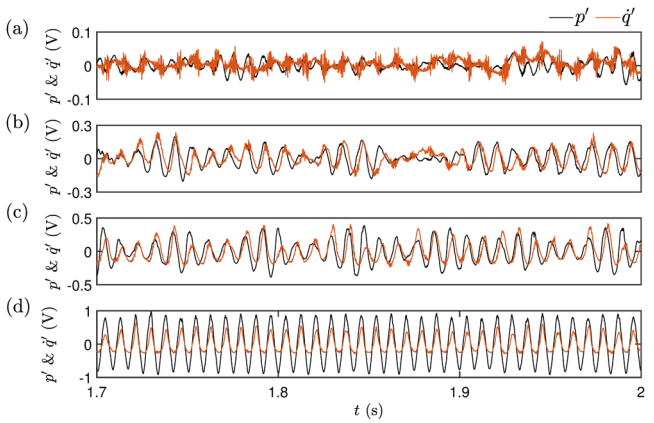


FIG. 1. [(a)–(d)] The time series of the acoustic pressure fluctuations (p') shown in black and unsteady heat release rate fluctuations ($\dot{q}'$) shown in red at mean flow velocities $\bar{u} = 9.2$, 11.9, 12.5, and 17.2 m/s, respectively.

Pawar *et al.*[25] used a measure of synchronization based on the recurrence behavior of the phase space trajectory of the signal, i.e., the plot of probability of recurrence $P(\tau)$ [Eq. (5)], to characterize the type of synchronization observed during the regimes shown in Fig. 1. They found that the signals are desynchronized during the state of combustion noise [Fig. 1(a)]. They described intermittency as the state of intermittent phase synchronization (IPS), where during the bursts of periodic oscillations, both signals are phase locked and during the aperiodic epochs, the signals are desynchronized. They reported that during the state of weakly correlated LCO, the signals are phase synchronized (PS) and during the state of strongly correlated LCO, the signals are in a state of generalized synchronization (GS).

Furthermore, we note that the construction of $P(\tau)$ plots is based on characterizing the recurrences in the phase space trajectories of the signal. Therefore, in order to analyze the coupled behavior of p' and $\dot{q}'$ signals, we plot recurrence plots obtained from *JRM* and *CRM* of these signals (shown in Fig. 2).

A. Analysis of synchronization transition using multivariate recurrence plots

A black dot in the joint recurrence plot (JRP) [Figs. 2(a)–2(d)] represents the presence of simultaneous recurrence in both p' and $\dot{q}'$ signals. During the desynchronized state, we observe irregular points in the JRP [Fig. 2(a)] as the time series of both p' and $\dot{q}'$ are aperiodic. The density of the black dots is low during the desynchronized state due to the lower occurrence of simultaneous recurrences in p' and $\dot{q}'$. During the IPS state, we observe discontinuous diagonal lines and irregular black patches [Fig. 2(b)], which is due to the presence of both weakly correlated limit cycle oscillations during epochs of bursts and low amplitude aperiodic regimes in p' and $\dot{q}'$, respectively. The presence of discontinuous diagonal lines in Fig. 2(c) is due to the weakly periodic nature of LCO observed during the PS state. During the GS state, as the signals exhibit strongly correlated LCO and as they share a functional relationship,[25] there are more occurrences of simultaneous recurrences. Hence, we observe continuous lines parallel to the main diagonal line [Fig. 2(d)]. From the JRP, we find that the occurrence of simultaneous recurrences in p' and $\dot{q}'$ increases with the onset of synchronization between p' and $\dot{q}'$.

Figures 2(e)–2(h) show the cross recurrence plots (CRPs) of p' and $\dot{q}'$. The choice of threshold for the cross recurrence rate (0.05) is lower than the threshold chosen for the individual recurrence rates (0.08) in order to distinguish the individual recurrence networks.[49] CRP encodes the information related to the presence of similar states in the phase space of the signals. During the GS state, there are similar states in both the signals, and hence, the CRP [Fig. 2(h)] looks similar to the JRP [Fig. 2(d)]. During the desynchronized state, the CRP is completely different from the individual RPs of p' and $\dot{q}'$, as the structures present in CRP [Fig. 2(e)] are different from that of JRP [Fig. 2(a)]. The occurrence of similar states is seen in the recurrence plots when there is synchronization between the signals. The appearance of

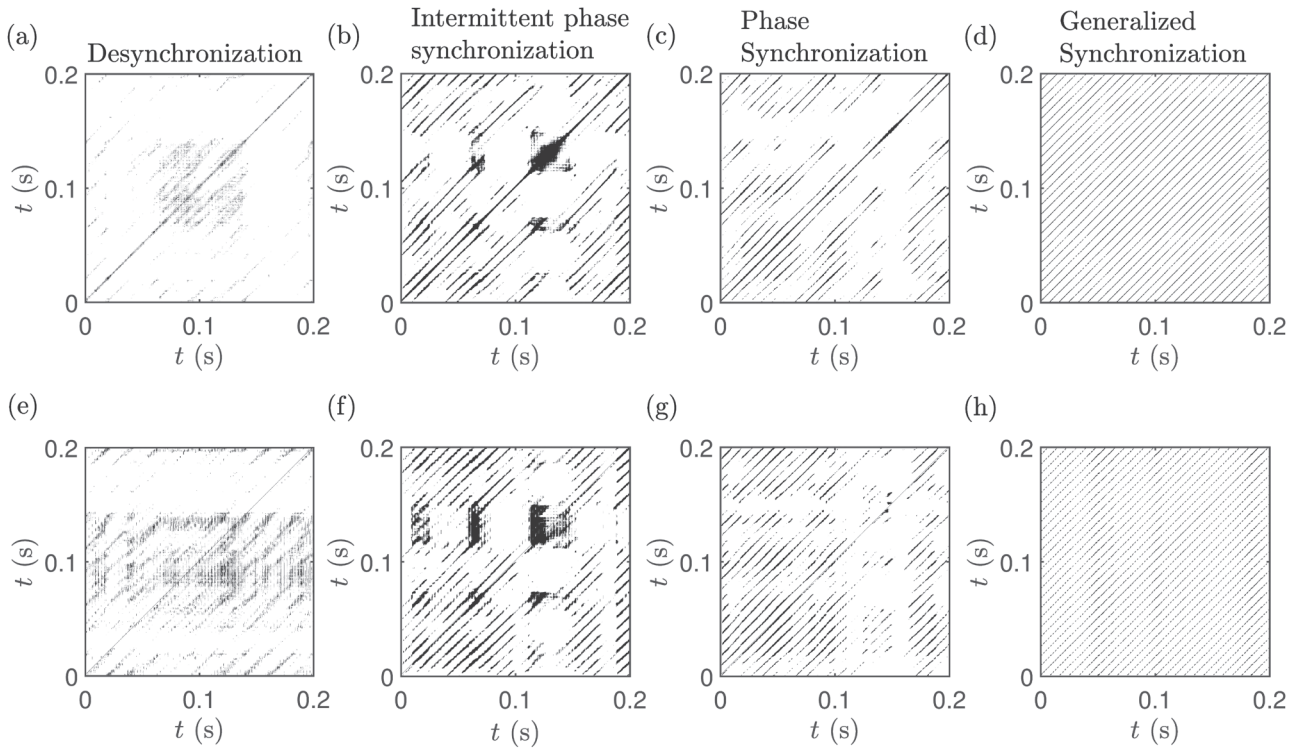


FIG. 2. [(a)–(d)] Joint recurrence plots (JRP) of p' and $\dot{q}'$ and [(e)–(h)] cross recurrence plots (CRP) of p' and $\dot{q}'$ for desynchronized, IPS, PS, and GS states, respectively. An embedding dimension of 6, a time delay of 2 ms, and a fixed recurrence rate of 0.08 is used for the computation of individual recurrence matrices, and a fixed recurrence rate of 0.05 is used for the computation of cross recurrence matrix.

these JRPs and CRPs in Fig. 2 is specific to our system in which we observe synchronization transition from an aperiodic state to a periodic state. These plots will appear differently for other systems where the synchronized state is not a periodic one.

As RP is a graphical tool for visualizing the dynamics of complex systems, the qualitative visual description of such plots can be quantified using measures from recurrence quantification analysis (RQA)[57,58] as given in Sec. II A. This quantification gives more objective results than a visual description. The plots of these measures are shown in Fig. 3.

Figure 3(a) shows the variation of DET_J [Eq. (6)] computed from the JRP of p' and $\dot{q}'$ with $\bar{u}$. We observe that DET_J becomes maximum and reaches a value closer to 1 during the occurrence of PS, as the signals observed during this state are weakly correlated LCO. Thus, DET_J can be used to detect the PS state whose dynamics is periodic, similar to that we have in our system. Figure 3(b) depicts the variation of RR of the joint recurrence matrix with $\bar{u}$. We observe that the value of RR_J [Eq. (10)] increases with $\bar{u}$. Due to the onset of synchronization, the simultaneous occurrence of recurrences in JRPs increases which leads to the increase in RR_J. We observe that RR_J is maximum during GS and is also able to detect the transition from the desynchronized state to the PS state. The transition to the PS state happens via the IPS state which results in the smooth change in RR_J. During the region of PS in the system dynamics, RR_J displays a plateau in the plot. This further indicates that the recurrence properties of both signals nearly remain the same, although the flow velocities are sufficiently increased during the PS state. During the transition from PS to GS, as the diagonal lines in JRP become more continuous [Fig. 2(d)] due to the increase in the recurrence behavior of trajectories, their mean RR_J values exhibit an increase in the plot [Fig. 3(b)].

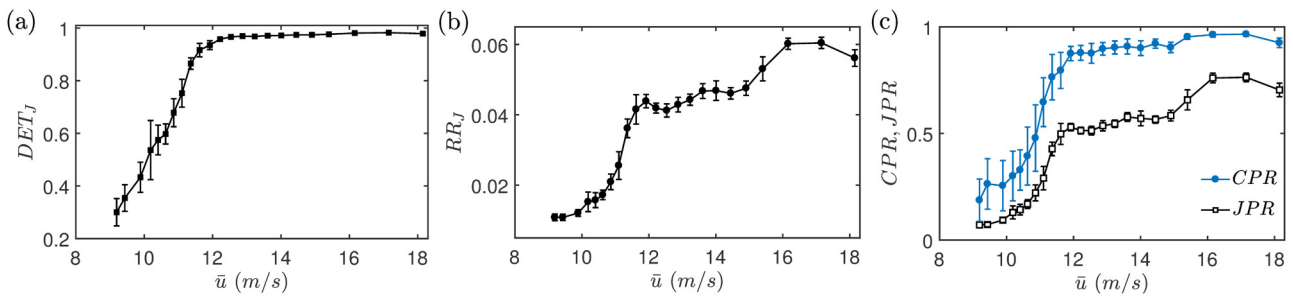


FIG. 3. [(a)–(c)] Variation of DET_J, RR_J, CPR, and JPR with $\bar{u}$, respectively. The properties are computed for an embedding dimension of 6, a time delay of 2 ms, and a fixed RR of 0.08. The signal of length 30 000 is divided into windows of length 3000, and the mean values of the properties are plotted. The error bars represent the standard deviation.

Figure 3(c) depicts the variation in *CPR* [Eq. (8)] and *JPR* [Eq. (9)] computed from the $P(\tau)$ plots of p' and $\dot{q}'$. We observe that the mean values of both *CPR* and *JPR* increase with increase in $\bar{u}$. During the PS state, as the location of peaks in $P(\tau)$ plots of the two signals matches,[25] *CPR* becomes closer to 1. Hence, it can be used to detect the PS state. We also observe that *CPR* shows only a slight change during the transition to GS. On the other hand, we observe that *JPR* reaches its maximum during GS and also is able to detect the transition from the PS to GS state. The presence of IPS between the desynchronized state and the PS state results in the smooth change of these measures.

We find that the measures computed using the recurrence plots and the $P(\tau)$ plots show the transition from the desynchronized state to PS and GS states and, hence, can be used as indices to detect the PS and GS states in thermoacoustic systems.

B. Detection of synchronization transition and directional dependence using recurrence networks

Now, we aim to detect the directionality of coupling that exists between p' and $\dot{q}'$ during different dynamical states. We construct joint and intersystem recurrence networks and compute network properties for this purpose.

Figures 4(a)–4(d) are the joint recurrence networks (JRNs) of p' and $\dot{q}'$ obtained during different states of combustion dynamics. The nodes are colored based on their degree, and the colorbar to the right indicates the variation of color with the degree of the node. We uncover that as the transition occurs from the desynchronized state [Fig. 4(a)] to the GS state [Fig. 4(d)] through the IPS state [Fig. 4(b)] and the PS state [Fig. 4(c)], the degree distribution becomes more uniform and concentrated toward lower degree (shown by blue color). During the desynchronized state [Fig. 4(a)], the color of the nodes varies from blue (lower degree) to red (higher degree). During the GS state in Fig. 4(d), the color of the nodes is almost the same and concentrated toward lower degree. The topology is similar to a limit cycle. This is a result of the occurrence of more simultaneous recurrences and the periodic nature of the signals during the GS state. During the IPS state [Fig. 4(b)], we observe that some part of the topology is similar to a limit cycle, whereas some part is similar to a chaotic structure. During bursts of periodic oscillations, the signals are phase synchronized and hence have simultaneous occurrence of recurrences and periodic dynamics. During the aperiodic regions, the signals are desynchronized, and we observe a chaotic structure in the network. We observe from Figs. 4(c) and 4(d) that during the PS state, the limit cycle is wider when compared with the GS state. This is due to the weakly correlated LCO exhibited during the PS state and the strongly correlated LCO observed during the GS state.

Figures 4(e)–4(h) show the network topologies of the individual recurrence networks of p' and $\dot{q}'$ along with the connections between them obtained for different states of combustion dynamics. The links with the orange color indicate the interconnections between the p' and $\dot{q}'$ networks obtained from the *CRM* computed using the Euclidean distance measured from the states in the phase space of p' to the states in the phase space of $\dot{q}'$ (i.e., $p' \rightarrow \dot{q}'$). The interlink represents the presence of a state in the same neighborhood of both the phase spaces, i.e., the interlink connects the nodes which correspond to the states that are similar to both p' and $\dot{q}'$.

During the desynchronized state [Fig. 4(e)], the networks of p' and $\dot{q}'$ are connected in an irregular fashion and the individual networks do not overlap. This is due to the presence of very few similar states. During the IPS state [Fig. 4(f)], some nodes of both networks (red and green color) in some regions are closer, while in some regions, they are farther apart. This is due to the phase locking behavior of both the signals during

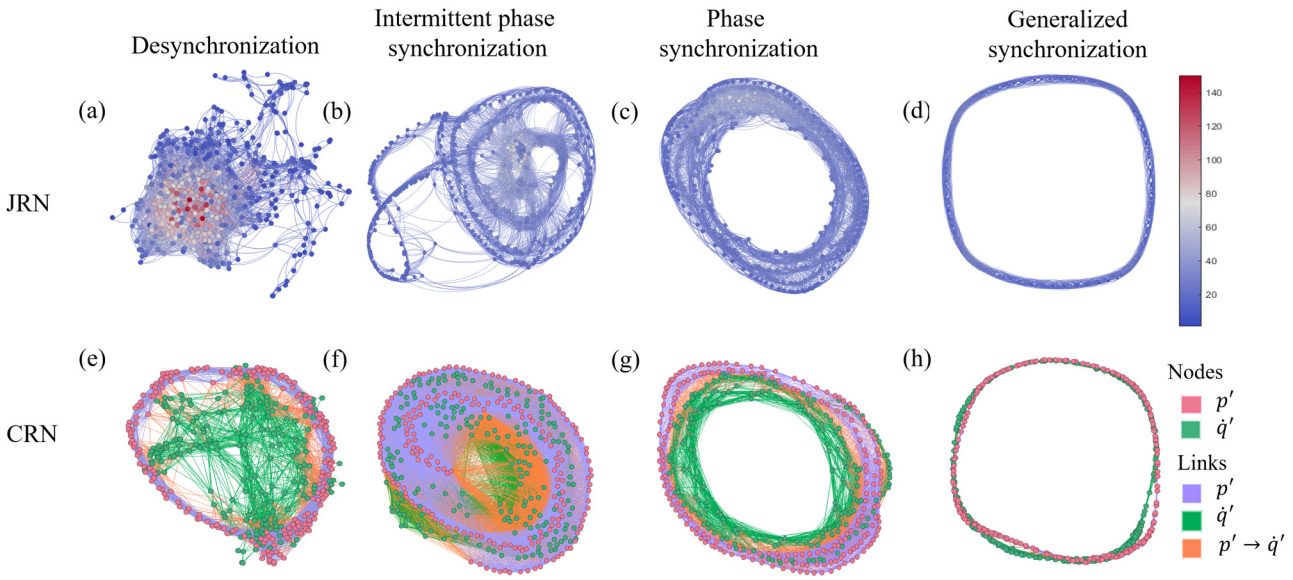


FIG. 4. [(a)–(d)] Topologies of the joint recurrence networks (JRN) constructed from the joint recurrence matrices and [(e)–(h)] topologies of the networks constructed from the intersystem recurrence networks with the interlinks based on the cross recurrence matrices (CRN) during desynchronized, IPS, PS, and GS states, respectively. The networks are constructed from 5000 data points with a fixed recurrence rate of 0.08 for individual recurrence matrices and 0.05 for the cross recurrence matrices. For the purpose of clear visualization, 500 nodes are considered for JRN and 200 nodes for each individual network in CRN. We use Force Atlas layout in Gephi software (https://gephi.org/) for network visualization.

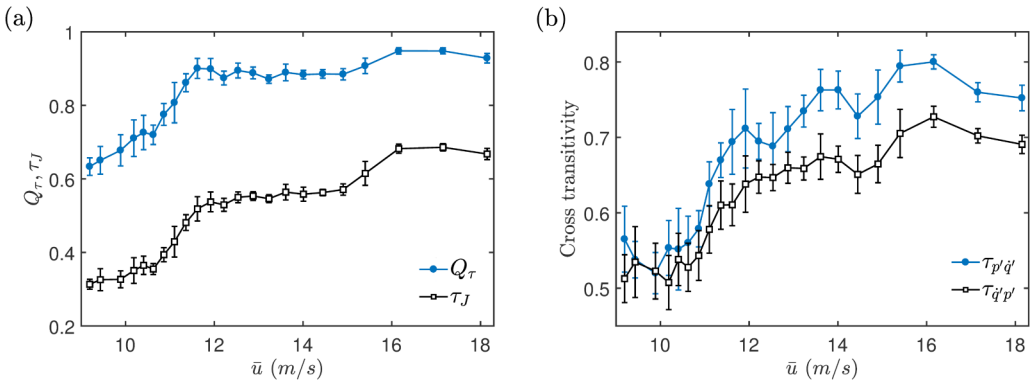


FIG. 5. (a) Variation of joint transitivity ($\mathcal{T}_J$) and transitivity ratio ($Q_\mathcal{T}$) of joint recurrence networks with $\bar{u}$. (b) Variation of cross transitivities ($\mathcal{T}_{p'\dot{q}'}, \mathcal{T}_{\dot{q}'p'}$) of the cross recurrence networks with $\bar{u}$. The networks are constructed from 5000 data points using an embedding dimension of 6, time delay of 2 ms, and a fixed *RR* of 0.08 for the individual recurrence networks and 0.05 for the cross recurrence networks. The signal of length 30 000 is divided into windows of length 3000, and the mean values of the properties are plotted. The error bars represent the standard deviation.

the bursts which results in the presence of similar states and the desynchronous behavior in the aperiodic parts of the signal. During the PS state [Fig. 4(g)], we observe that the individual networks and the interconnections form a thicker limit cycle, whereas the width of this topology becomes less during the GS state [Fig. 4(f)], and hence, the individual networks appear much closer to each other. The proximity and overlap between the individual networks observed during the GS state indicate the presence of similar states.

We use a network measure, transitivity obtained from both joint and intersystem recurrence matrices, to quantify the synchronization transition in the system. Figure 5(a) shows the variation of joint transitivity ($\mathcal{T}_J$—blue color) [Eq. (12)] and transitivity ratio ($Q_\mathcal{T}$—red color) [Eq. (13)] with $\bar{u}$. We see that $\mathcal{T}_J$ increases with $\bar{u}$ and reaches its maximum value during the GS state. Due to the presence of similar states during GS, the individual transitivities will be similar to that of $\mathcal{T}_J$. Thus, the normalized measure, $Q_\mathcal{T}$, reaches a maximum value around 1 during GS. Hence, $Q_\mathcal{T}$ can be used as an index to detect the GS state, and both the measures, $\mathcal{T}_J$ and $Q_\mathcal{T}$, can be used to detect the synchronization transition. The smooth increase in these measures from the desynchronized state to the PS state is due to the presence of the IPS state.

Figure 5(b) shows the variation in cross transitivities $\mathcal{T}_{p'\dot{q}'}$, $\mathcal{T}_{\dot{q}'p'}$ with $\bar{u}$. Here, $\mathcal{T}_{p'\dot{q}'}$ is the probability that two nodes in the recurrence network of $\dot{q}'$ are connected given that they are neighbors to a node in the recurrence network of p'. The interconnections between p' and $\dot{q}'$ are identified using the CRP from $p' \rightarrow \dot{q}'$. As the *CRM* is not necessarily symmetric, the interconnections can differ based on whether the distance matrix is computed from $p' \rightarrow \dot{q}'$ or from $\dot{q}' \rightarrow p'$. Due to the differences in the interconnections, the cross transitivity need not be symmetric and hence can be used as an indicator of directionality between the signals of coupled oscillators. The differences in the cross transitivity can be due to the way in which the individual systems are coupled.[49] We observe that during the states of desynchronization and IPS, both $\mathcal{T}_{p'\dot{q}'}$ and $\mathcal{T}_{\dot{q}'p'}$ have nearly the same value, as the coupling between p' and $\dot{q}'$ is weak. During the PS state, we observe that $\mathcal{T}_{p'\dot{q}'}$ is higher than $\mathcal{T}_{\dot{q}'p'}$, which might happen due to a stronger influence of $\dot{q}'$ on p' than vice versa. We know that there is a mutual coupling between p' and $\dot{q}'$ during the state of thermoacoustic instability. Thus, the difference between $\mathcal{T}_{p'\dot{q}'}$ and $\mathcal{T}_{\dot{q}'p'}$ observed in Fig. 5(b) may be due to an asymmetric bidirectional coupling between p' and $\dot{q}'$ with a stronger influence of $\dot{q}'$ on p' than vice versa. In most systems which undergo synchronization transition, we do not see a growth in amplitude like in our case.[59] This results in a speculation that the dynamics observed in our system can be due to parametric resonance and need not be synchronization. However, if the dynamics were a result of resonance, there should not be any asymmetry in the coupling between p' and $\dot{q}'$, which we discovered in our system. This reaffirms that the transition to thermoacoustic instability is indeed due to the synchronization between p' and $\dot{q}'$.

V. CONCLUSIONS

We quantified the synchronization transition of the acoustic pressure (p') and the unsteady heat release rate ($\dot{q}'$) fluctuations in a thermoacoustic system using measures derived from multivariate recurrence plots and recurrence networks. Furthermore, we demonstrated that the measures, determinism (*DET*) and correlation of probability of recurrence (*CPR*) can be used to detect the occurrence of the state of phase synchronization (PS), and the measures, recurrence rate (*RR*) and joint probability of recurrence (*JPR*), can be used to detect the occurrence of generalized synchronization state (GS). We constructed the joint recurrence networks and the cross recurrence networks from the corresponding time series and found that the network properties, namely, joint transitivity ($\mathcal{T}_J$) and transitivity ratio ($Q_\mathcal{T}$), are efficient indices to detect GS. Furthermore, in order to characterize the directionality of coupling between p' and $\dot{q}'$, we used cross transitivity. We discovered a possible asymmetric bidirectional coupling between p' and $\dot{q}'$ during the PS and GS states. We observed that $\dot{q}'$ exerts a greater influence on p' than vice versa. This directional dependence will be crucial in designing effective control mechanisms and modeling the system behavior during thermoacoustic instability. In our system, as we observed that the heat release rate has a stronger influence on acoustic

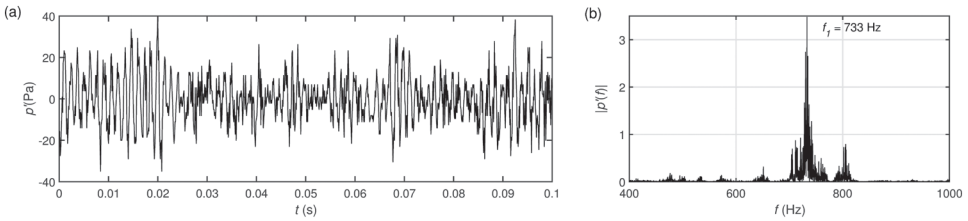


FIG. 6. [(a) and (b)] The time series and the amplitude spectrum of the acoustic pressure signal acquired during the cold conditions with the air flow velocity of 9.1 m/s, respectively. In the presence of a turbulent flow, the amplitude spectrum shows a sharp peak at $f_1 = 733$ Hz, which is an indicative of correlated self-sustained oscillations in the signal.

pressure, a control on the flame might possibly be more efficient than a control on the acoustic field in order to prevent thermoacoustic instability.

ACKNOWLEDGMENTS

This work has been financially supported by the German Research Foundation (DFG Project No. MA4759/9). We would like to thank the Office of Naval Research (ONR) Global for the financial support and Contract monitor: Dr. Ramesh Kolar (Grant No. N62909-18-1-2061). We gratefully acknowledge DAAD for funding the lead author to pursue internship with Dr. Norbert Marwan and Professor Jürgen Kurths. We acknowledge DST-DAAD (Order No. DST/INT/FRG/DAAD/P-12/2017) for supporting this Indo-German collaboration. We are grateful to Professor Wolfgang Polifke and Dr. Thomas Komarek for giving us their swirl combustor design based on which our bluff body combustor is designed. We express our gratitude to Dr. K. P. Harikrishnan of Cochin College, Professor G. Ambika of IISER, Tirupathi, and Professor R. Misra of IUCAA, Pune for the valuable suggestions which helped us a lot in improving the draft.

APPENDIX: ACOUSTIC FIELD AND UNSTEADY HEAT RELEASE RATE FLUCTUATIONS IN A TURBULENT COMBUSTOR ARE SELF-SUSTAINED OSCILLATORS

In order to prove that the acoustic field in a duct with a turbulent flow is a self-sustained oscillator, we perform separate experiments on the same experimental setup (used in the present study) in the cold flow environment by removing the flame and maintaining the same flow conditions. Figures 6(a) and 6(b) show the time series and the amplitude spectrum of the pressure signal acquired for the air flow condition of 9.1 m/s, respectively. We observe a dominant peak at 733 Hz, compared to the other low magnitude frequency peaks in the spectrum [Fig. 6(b)]. Furthermore, the existence of a dominant frequency in the spectrum indicates the presence of correlations in the signal, which is different from the characteristics of noise. This affirms that for turbulent flows confined in a duct, from the viewpoint of oscillation theory, acoustic pressure is a self-sustained oscillator with seemingly chaotic fluctuations.

Furthermore, various studies have been conducted on open turbulent flames in the past. Turbulent flows cause oscillations in the flame front that, in turn, cause fluctuations in the flame surface area and hence fluctuations in the heat release rate. Several studies showed that sound pressure levels (SPL) of combustion noise produced by open turbulent jet flames exhibit a broadband spectrum concentrated at lower frequencies.[60–63] Thus, uncoupled turbulent flames with the acoustic field can behave like a self-sustained oscillator with aperiodic fluctuations.

Thus, under the influence of a turbulent flow, the acoustic field and the heat release rate in the combustor can be considered as self-sustained aperiodic oscillators. Each of these oscillators is otherwise damped oscillators; however, the presence of continuous perturbations from the inherent turbulent hydrodynamic flow makes them self-sustained oscillators. Thus, the synchronization framework can be applied to study the onset of thermoacoustic instability in a turbulent combustor.

Furthermore, in the combustor, these oscillators are not distinct but are inherently coupled with each other through the medium of the turbulent flow field. Similar behavior can be seen in complex biological systems such as human respiratory system, where synchronization between cardiovascular and respiratory systems is considered, even though these subsystems cannot be considered as independent.[64] This is because a weak coupling between these systems is observed, and it also has been reported that these systems are generally not phase-locked. Analogously, in a complex system such as ours, during combustion noise, the acoustic pressure and unsteady heat release rate are desynchronized. This desynchronized behavior can be due to the weak coupling between the turbulent reactive flows and the combustor acoustics. During the transition to thermoacoustic instability, the coupling between these subsystems gradually enhances, leading to a generalized synchronization state.

[1]T. C. Lieuwen, J. Propul. Power **18**, 61 (2002).
[2]A. M. Annaswamy, M. Flefil, J. P. Hathout, and A. F. Ghoniem, Combust. Sci. Tech. **128**, 131 (1997).
[3]R. I. Sujith, M. P. Juniper, and P. J. Schmid, Int. J. Spray Combust. Dyn. **8**, 119 (2016).
[4]F. E. Culick, in *Modern Research Topics in Aerospace Propulsion*, edited by G. Angelino, L. De Luca, and W. A. Sirignano (Springer, New York, 1991).
[5]P. G. M. Hoeijmakers, Ph.D. thesis, Dutch Institute of Systems and Control, 2014.
[6]F. E. Culick and P. Kuentzmann, NATO Research and Technology Organization, 2006.
[7]T. C. Lieuwen and V. Yang, *Combustion Instabilities in Gas Turbine Engines: Operational Experience, Fundamental Mechanisms, and Modeling* (American Institute of Aeronautics and Astronautics, 2005).
[8]V. Nair, G. Thampi, and R. I. Sujith, J. Fluid Mech. **756**, 470 (2014).
[9]M. Murugesan and R. I. Sujith, J. Propul. Power **32** ,707 (2016).
[10]H. Gotoda, Y. Shinoda, M. Kobayashi, and Y. Okuno, Phys. Rev. E **89**, 022910 (2014).
[11]W. Lang, T. Poinsot, and S. Candel, Combust. Flame **70**, 281 (1987).
[12]S. Candel, Proc. Combust. Inst. **24**, 1277 (1992).
[13]K. R. McManus, T. Poinsot, and S. Candel, Prog. Energy Combust. Sci. **16**, 1 (1993).
[14]J. P. Hathout, A. M. Annaswamy, M. Fleifil, and A. F. Ghoniein, Combust. Sci. Tech. **132**, 99 (1998).

[15]F. E. C. Culick, Acta Astron. **3**(9), 715 (1976).
[16]M. P. Juniper and R. I. Sujith, Ann. Rev. Fluid Mech. **50**, 661 (2018).
[17]A. P. Dowling, J. Fluid Mech. **346**, 271 (1997).
[18]H. Gotoda, H. Nikimoto, T. Miyano, and S. Tachibana, Chaos **21**, 013124 (2011).
[19]F. E. C. Culick, AIAA J. **32**(1), 146 (1994).
[20]L. Kabiraj, R. I. Sujith, and P. Wahi, J. Eng. Gas Turbine Power **134**, 031502 (2012).
[21]L. Kabiraj, A. Saurabh, P. Wahi, and R. I. Sujith, Chaos **22**, 023129 (2012).
[22]S. Mondal, V. R. Unni, and R. I. Sujith, J. Fluid Mech. **811**, 659 (2017).
[23]N. B. George, V. R. Unni, M. Ragunathan, and R. I. Sujith, Int. J. Spray Combust. Dyn. 1 (2018).
[24]S. A. Pawar and R. I. Sujith, J. Combust. Soc. Jpn. **60**(192), 99 (2018).
[25]S. A. Pawar, A. Seshadri, V. R. Unni, and R. I. Sujith, J. Fluid. Mech. **827**, 664 (2017).
[26]V. Nair, G. Thampi, and R. I. Sujith, Int. J. Spray Combust. Dyn. **5**, 273 (2013).
[27]J. Tony, E. A. Gopalakrishnan, E. Sreelekha, and R. I. Sujith, Phys. Rev. E **92**, 062902 (2015).
[28]V. Nair and R. I. Sujith, J. Fluid Mech. **747**, 635 (2014).
[29]V. R. Unni and R. I. Sujith, J. Fluid Mech. **784**, 30 (2015).
[30]V. R. Unni, A. Mukhopadhya, and R. I. Sujith, Int. J. Spray Combust. Dyn. **7**(3), 243 (2015).
[31]M. Murugesan and R. I. Sujith, J. Fluid Mech. **772**, 225 (2015).
[32]H. Gotoda, H. Kinugawa, R. Tsujimoto, S. Domen, and Y. Okuno, Phys. Rev. Appl. **7**, 044027 (2017).
[33]V. Godavarthi, V. R. Unni, E. A. Gopalakrishnan, and R. I. Sujith, Chaos **27**, 063113 (2017).
[34]J. S. W. Rayleigh, Nature **18**(455), 319 (1878).
[35]D. E. Rogers, Jet Propul. **26**(6), 456 (1956).
[36]J. O. Keller, L. Vaneveld, D. Korschelt, G. L. Hubbardd, A. F. Ghoniem, J. W. Daily, and A. K. Oppenheim, AIAA J. **20**(2), 254 (1982).
[37]D. A. Smith and E. E. Zukoski, in *AIAA/SAE/ASME/ASEE 21st Joint Propulsion Conference*, AIAA Paper No. 85-1248 (AIAA, 1985).
[38]D. A. Smith and E. E. Zukoski, in *AIAA 25th Aerospace Sciences Meeting*, AIAA-87-0220 (AIAA, 1987).
[39]T. J. Poinsot, A. C. Trouve, D. P. Veynante, S. M. Candel, and E. J. Espito, J. Fluid Mech. **177**, 265 (1987).
[40]H. K. Yu, A. Trouve, and J. W. Daily, J. Fluid Mech. **232**, 47 (1991).
[41]M. A. Macquisten and A. P. Dowling, Combust. Flame **94**(3), 253 (1993).
[42]J. C. Broda, S. Seo, R. J. Santoro, G. Shirhattikar, and V. Yang, Proc. Combust. Inst. **27**(2), 1849 (1998).
[43]K. K. Venkataraman, L. H. Preston, D. W. Simons, B. J. Lee, J. G. Lee, and D. A. Santavicca, J. Propul. Power **15**(6), 909 (1999).
[44]F. Guethe and B. Schuermans, Meas. Sci. Technol. **18**(9), 3036 (2007).
[45]R. Sivakumar and S. R. Chakravarthy, Int. J. Aeroacoust. **7**(34), 267 (2008).
[46]S. Chiocchini, T. Pagliaroli, and R. Camussi, J. Propul. Power **34**(1), 15 (2018).
[47]M. C. Romano, M. Thiel, J. Kurths, I. Z. Kiss, and J. L. Hudson, Europhys. Lett. **71**(3), 466 (2005).
[48]J. H. Feldhoff, R. V. Donner, J. F. Donges, N. Marwan, and J. Kurths, Europhys. Lett. **102**, 30007 (2013).
[49]J. H. Feldhoff, R. V. Donner, J. F. Donges, N. Marwan, and J. Kurths, Phy. Lett. A **376**(46), 3504 (2012).
[50]J. P. Eckmann, S. O. Kamphorst, and D. Ruelle, Europhys. Lett. **4**, 973 (1987).
[51]F. Takens, *Lecture Notes in Mathematics* (Springer, Heidelberg, 1981), Vol. 898.
[52]L. Cao, Phys. D **110**, 43 (1997).
[53]M. C. Romano, M. Thiel, J. Kurths, and W. von Bloh, Phys. Lett. A **330**, 214 (2004).
[54]B. Goswami, G. Ambika, N. Marwan, and J. Kurths, Physica A **391**, 4364 (2012).
[55]N. Marwan, J. F. Donges, Y. Zou, R. V. Donner, and J. Kurths, Phys. Lett. A **373**, 4246 (2009).
[56]M. E. J. Newman, SIAM Rev. **45**, 167 (2003).
[57]C. L. Webber, Jr and J. P. Zbilut, J. Appl. Physiol. **76**(2), 965 (1994).
[58]N. Marwan, N. Wessel, U. Meyerfeldt, A. Schirdewan, and J. Kurths, Phys. Rev. E **66**(2), 026702 (2002).
[59]A. Balanov, N. Janson, D. Postnov, and O. Sosnovtseva, *Synchronization: From Simple to Complex* (Springer, Berlin, 2009).
[60]B. N. Shivashankara, W. C. Strahle, and J. C. Handley, AIAA Conf. **37**, 277 (1973).
[61]W. C. Strahle, Prog. Energ. Combust. **4**, 157 (1978).
[62]W. C. Strahle and J. I. Jagoda, Symp. (Int.) Combust. **22**, 561 (1989).
[63]R. Rajaram and T. Lieuwen, J. Fluid. Mech. **637**, 357 (2009).
[64]C. Schäfer, M. G. Rosenblum, H.-H. Abel, and J. Kurths, Phys. Rev. E **60**, 857 (1999).